












Article

Abietane Diterpenes from *Medusantha martusii* and Their Anti-Neuroinflammatory Activity

Edileuza B. de Assis ¹, Rodrigo S. de Andrade ¹, Joanda P. R. e Silva ¹, Lucas H. Martorano ², Geraldo M. W. Amorim ¹, Paulo B. A. Loureiro ¹, Lucas S. Abreu ², Marianna V. Sobral ¹, Marcus T. Scotti ¹, Fernando M. dos Santos Junior ², Maria de Fátima Agra ¹, Josean F. Tavares ^{1,*} and Marcelo S. da Silva ^{1,*}

- ¹ Postgraduate Program in Natural and Synthetic Bioactive Products, Federal University of Paraíba, João Pessoa 58051-900, Brazil; edileuzabezerra@ltf.ufpb.br (E.B.d.A.); rodrigo@ltf.ufpb.br (R.S.d.A.); joandapaolla.1@gmail.com (J.P.R.e.S.); moiseswand@ltf.ufpb.br (G.M.W.A.); paulobrunoaloureiro@ltf.ufpb.br (P.B.A.L.); mariannavbs@gmail.com (M.V.S.); mtscotti@ccae.ufpb.br (M.T.S.); agramf@ltf.ufpb.br (M.d.F.A.)
- ² Department of Organic Chemistry, Fluminense Federal University, Niterói 24020-141, Brazil; lucashm@id.uff.br (L.H.M.); abreu_lucas@id.uff.br (L.S.A.); fernando_martins@id.uff.br (F.M.d.S.J.)
- * Correspondence: josean@ltf.ufpb.br (J.F.T.); marcelosobral@ltf.ufpb.br (M.S.d.S.)

Abstract: Seven new abietane diterpenoids, comprising medusanthol A–G (1–3, 5, 7–9) and two previously identified analogs (4 and 6), were isolated from the hexane extract of the aerial parts of *Medusantha martusii*. The structures of the compounds were elucidated by HRESIMS, 1D/2D NMR spectroscopic data, IR spectroscopy, NMR calculations with DP4+ probability analysis, and ECD calculations. The anti-neuroinflammatory potential of compounds 1–7 was evaluated by determining their ability to inhibit the production of nitric oxide (NO) and the proinflammatory cytokine TNF- α in BV2 microglia stimulated with LPS and IFN- γ . Compounds 1–4 and 7 exhibited decreased NO levels at a concentration of 12.5 μ M. Compound 1 demonstrated strong activity with an IC₅₀ of 3.12 μ M, and compound 2 had an IC₅₀ of 15.53 μ M; both compounds effectively reduced NO levels compared to the positive control quercetin (IC₅₀ 11.8 μ M). Additionally, both compounds significantly decreased TNF- α levels, indicating their potential as promising anti-neuroinflammatory agents.

Keywords: *Medusantha martusii*; Caatinga; diterpenes; aromatic abietane; neurodegenerative diseases; TNF- α



Citation: Assis, E.B.d.; Andrade, R.S.d.; Silva, J.P.R.e.; Martorano, L.H.; Amorim, G.M.W.; Loureiro, P.B.A.; Abreu, L.S.; Sobral, M.V.; Scotti, M.T.; Santos Junior, F.M.d.; et al. Abietane Diterpenes from *Medusantha martusii* and Their Anti-Neuroinflammatory Activity. *Molecules* **2024**, *29*, 2723. <https://doi.org/10.3390/molecules29122723>

Academic Editor: Seyed Khosrow Tayebati

Received: 10 May 2024
Revised: 23 May 2024
Accepted: 27 May 2024
Published: 7 June 2024



Copyright: © 2024 by the authors. Licensee MDPI, Basel, Switzerland. This article is an open access article distributed under the terms and conditions of the Creative Commons Attribution (CC BY) license (<https://creativecommons.org/licenses/by/4.0/>).

1. Introduction

The Lamiaceae family, which consists of plants and shrubs, is composed of approximately 258 genera and 7193 species. In Brazil, over 500 species from the Lamiaceae family are distributed across 46 genera, with nearly half of these species belonging to the subfamily Nepetoideae [1,2], which is a well-known source of abietane-type diterpenoids [3,4]. The broad spectrum of biological activities associated with these compounds has garnered special attention, with many demonstrating anti-inflammatory [5], anticancer [6], antimicrobial [7], and antiprotozoal [8] properties.

Medusantha martusii (Benth.) Harley and J. F. B. Pastore (syn: *Hyptis martusii*), commonly known as “cidreira brava” or “cidreira-do-campo,” is a shrub native and endemic to Brazil and belongs to the subfamily Nepetoideae. This species is predominantly found in the Northeast region, specifically in the Caatinga, a unique semiarid biome exclusive to Brazil. In traditional Brazilian medicine, the infusion or decoction of *M. martusii* leaves is used to combat intestinal and stomach disorders, while the decoction of roots is commonly used to combat inflammation of the ovaries [9,10]. Previous phytochemical investigations of *M. martusii* have documented the isolation of abietane diterpenes from its roots and aerial parts, as well as the phytochemical profiling of its essential oil and its pharmacological activities [11–14]. However, to the best of our knowledge, there is no evidence in the

literature with respect to the anti-inflammatory activity of the isolated compounds. As part of our investigation into species from the Brazilian semiarid region, we conducted a chemical reinvestigation of *M. martiusii*, which led to the isolation of nine abietane diterpenes, including seven previously undescribed compounds named medusanthol A–G (1–3, 5, 7–9) and two known analogs (4 and 6). Here, we describe the isolation, structural elucidation, and anti-neuroinflammatory activity of these isolates.

2. Results and Discussion

2.1. Structure Elucidation of the Compounds

The hexanic extract of the aerial parts was fractionated into six fractions by vacuum liquid chromatography. The EtOAc fraction was purified using HPLC, yielding seven previously unknown (1–3, 5, 7–9) and two known (4 and 6) abietanes (Figure 1).

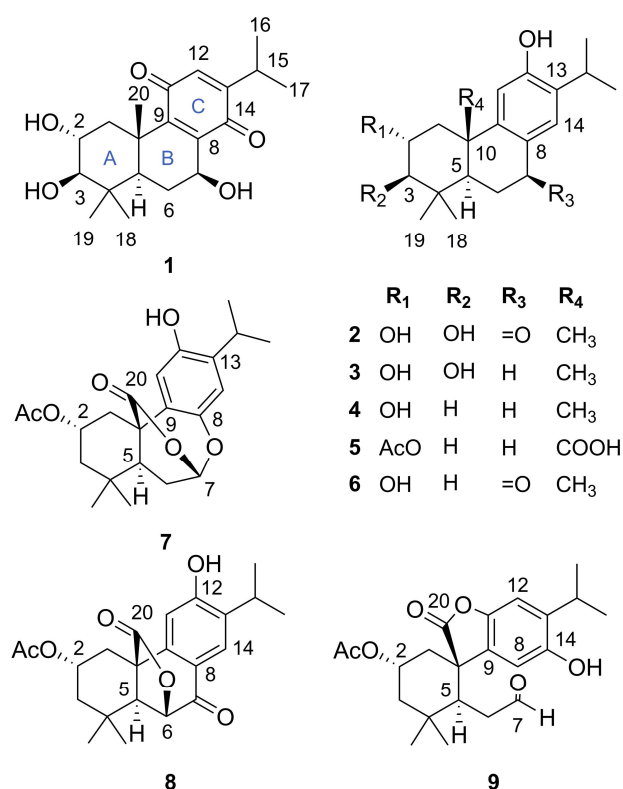


Figure 1. Chemical structures of the isolated abietanes 1–9.

Compound 1 was isolated as an amorphous brown powder and assigned the molecular formula $C_{20}H_{28}O_5$ based on its HRESIMS ion at m/z 331.1896 ($[M - H_2O + H]^+$, calcd for $C_{20}H_{27}O_4$, 331.1904, $\Delta = 2.2$ ppm), corresponding to seven degrees of hydrogen deficiency. The IR spectrum displayed absorption bands for hydroxy (3363 cm^{-1}) and conjugated keto carbonyl (1706 and 1645 cm^{-1}) groups. The ^{13}C NMR (Table 1) spectrum exhibited resonances for 20 carbons, including signals for two conjugated carbonyls at δ_C 188.0 and 190.1 and four olefinic carbons (three non-hydrogenated at δ_C 141.9, 150.6, and 153.6, and one hydrogenated at δ_C 132.4), consistent with the presence of a *para*-benzoquinone unit [15]. With the aid of the HSQC experiment, the remaining signals were assigned to five methyl carbons (δ_C 21.5, 21.4, 28.8, 17.0, 21.1), two methylene carbons (δ_C 42.3, 26.1), five methine carbons (including three sp^3 oxymethine at δ_C 82.8, 68.8, and 67.9 and one nonoxygenated sp^3 methine at δ_C 48.3), and two quaternary carbons (δ_C 38.9, 40.0). An analysis of 1H NMR data (Table 2) revealed the presence of an isopropyl group connected to *para*-benzoquinone through the signals of a methine hydrogen at δ_H 2.97 (1H, m, H-15) and two methyl groups at δ_H 1.10 and 1.08 (6H, s, H₃-16/H₃-17) [12]. Similarly, signals

for three oxymethine hydrogens at δ_{H} 4.79 (1H, dd, $J = 10.2, 7.5$ Hz, H-7), δ_{H} 3.01 (1H, d, $J = 9.6$ Hz, H-3), and δ_{H} 3.82 (1H, ddd, $J = 11.5, 9.6, 4.4$ Hz, H-2) were observed, as shown in Table 1. Based on the HSQC spectrum, the signal at δ_{H} 6.36 (1H, d, $J = 1.2$ Hz, H-12) was attributed to the olefinic hydrogen of the *para*-benzoquinone unit, the signals for methylene hydrogens at δ_{H} 1.15 (1H, m) and 3.06 (1H, dd, $J = 12.7, 4.4$ Hz) were assigned to H₂-1, and δ_{H} 2.20 (1H, m) and 1.64 (1H, m) were assigned to H₂-6. The aforementioned evidence suggests that compound 1 is an abietane quinone. In the HMBC spectrum, the correlations of the signal at δ_{H} 1.40 (3H, s) with the carbons at δ_{C} 42.3, 48.3, and 150.6 defined the methyl group CH₃-20 and the chemical shifts of carbons C-1, C-5, and C-9, respectively (Figure 2).

Table 1. ¹³C NMR data of compounds 1–3, 5, and 7–9.

No.	1 ^a	2 ^b	3 ^b	5 ^b	7 ^a	8 ^a	9 ^a
1	42.3	45.6	46.6	43.0	36.8	32.0	40.0
2	68.8	69.4	70.0	70.8	67.9	67.3	66.4
3	82.8	83.5	84.3	47.7	45.3	43.6	46.1
4	38.9	40.5	40.5	35.8	36.3	34.0	36.3
5	48.3	50.3	51.5	53.2	50.6	59.5	45.7
6	26.1	36.6	20.4	19.6	26.7	81.4	41.8
7	67.9	200.6	31.1	30.5	95.4	189.1	199.5
8	141.9	123.7	126.5	128.7	145.8	121.8	110.2
9	150.6	157.2	148.0	139.1	121.7	143.8	128.3
10	40.0	39.9	39.5	49.5	47.3	49.2	53.1
11	188.0	110.6	111.6	112.4	112.3	111.0	146.6
12	132.4	162.6	153.4	153.5	148.1	159.1	108.6
13	153.6	135.2	133.8	135.3	136.7	136.1	137.1
14	190.1	127.3	127.4	128.2	117.3	128.2	150.2
15	26.4	27.9	27.7	27.9	26.8	27.0	27.4
16	21.5	22.8	23.3	23.1	22.3	22.3	22.5
17	21.4	22.9	23.2	23.2	22.2	22.4	22.8
18	28.8	28.6	29.4	32.6	30.8	31.4	33.3
19	17.0	16.9	17.4	21.5	20.8	22.7	22.0
20	21.1	24.6	26.3	179.0	170.9	176.0	177.9
2-OCOCH ₃	-	-	-	21.4	21.3	21.4	21.4
2-OCOCH ₃	-	-	-	172.6	169.9	170.0	170.3

^a Recorded in CDCl₃, 125 MHz; ^b recorded in methanol-*d*₄, 100 MHz.

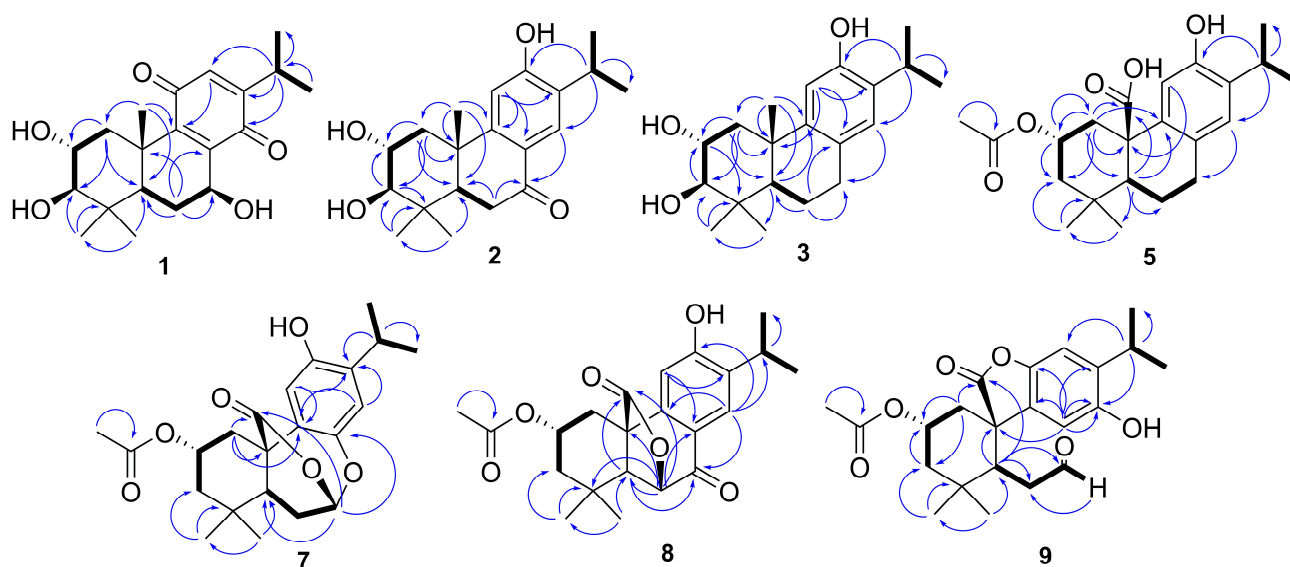


Figure 2. Key ¹H–¹H COSY (—) and HMBC (—) of compounds 1–3, 5, and 7–9.

Table 2. ^1H NMR data of compounds **1–3**, **5**, and **7–9** (J in Hz).

No.	1 ^a	2 ^b	3 ^b	5 ^b	7 ^c	8 ^c	9 ^c
1	1.15, m 3.06, dd (12.7, 4.4)	1.56, t (11.9) 2.55, dd (12.5, 4.3)	1.40, t (12.0) 2.49, dd (12.4, 4.4)	1.27, overlap 3.09, ddd (12.1, 4.5, 2.8)	1.85, t (11.7) 2.77 ddd (11.8, 3.7, 2.4)	1.76, t (12.0) 3.01, dd (12.6, 4.3)	1.71, dd (13.2, 11.7) 2.23, ddd (13.3, 4.0, 2.5)
2	3.82, ddd (11.5, 9.6, 4.4)	3.83, ddd (11.7, 9.6, 4.3)	3.78, ddd (11.6, 9.6, 4.4)	5.42, tt (11.7, 4.5)	5.22, tt (11.5, 3.9)	5.04, tt (11.6, 4.1)	5.50, tt (11.7, 3.9)
3	3.01, d (9.6)	3.02, d (9.6)	2.99, d (9.6)	1.86, overlap 1.27, overlap	1.14–1.23, m 1.97, ddd (12.4, 4.1, 2.4)	1.88, m 1.24, overlap	2.03, ddd (12.7, 4.0, 2.5) 1.49, t (12.3)
5	1.15, m	1.89, dd (13.4, 4.2)	1.32, dd (12.4, 2.4)	1.50, dd (12.8, 2.4)	2.15, dd (10.5, 2.0) 2.24 ddd (15.9, 6.5, 2.0)	2.41, s	2.34, dd (6.1, 4.6) 2.46, ddd (17.8, 4.6, 1.5)
6	2.20, m 1.64, m	2.64, m 2.64, m	1.84, m 1.71, m	2.54, m 1.86, overlap	2.35 dd (15.9, 10.5)	4.77, s	1.94, ddd (17.8, 6.1, 1.5)
7	4.79, dd (10.2, 7.5)	-	2.71, m 2.82, m	2.87, m 2.76, m	5.94 d (6.5)	-	9.19, t (1.5)
8	-	-	-	-	-	-	6.57, s
11	-	6.76, s	6.65, s	6.68, s	6.69, s	6.71, s	-
12	6.36, d (1.2)	-	-	-	-	-	6.86, s
14	-	7.80, s	6.75, s	6.85, s	6.70, s	7.91, s	-
15	2.97, m	3.22, sept (6.8)	3.16, sept (6.8)	3.18, sept (6.8)	3.08, sept (6.8)	3.16, sept (6.8)	3.16, sept (6.9)
16	1.10, s	1.19, d (6.8)	1.16, d (6.8)	1.17, d (6.8)	1.18, d (6.8)	1.23, s	1.20, d (6.9)
17	1.08, s	1.21, d (6.8)	1.15, d (6.8)	1.17, d (6.8)	1.19, d (6.8)	1.24, s	1.18, d (6.9)
18	1.07, s	1.06, s	1.07, s	1.02, s	0.86, s	1.07, s	0.94, s
19	0.91, s	0.98, s	0.89, s	0.93, s	0.96, s	1.05, s	1.23, s
20	1.40, s	1.27, s	1.19, s	-	-	-	-
2-	-	-	-	2.02, s	2.05, s	2.06, s	1.99, s
OCOCH ₃	-	-	-	-	-	-	-

^a Recorded in CDCl₃, 400 MHz; ^b recorded in methanol-*d*₄, 400 MHz; ^c recorded in CDCl₃, 500 MHz.

Furthermore, the correlations of the signals at δ_{H} 1.07 and 0.91 (6H, s, H₃-18/H₃-19) with the carbon signals at δ_{C} 38.9, 82.8, and 48.3 identified the two geminal methyl groups linked to C-4 and defined the chemical shifts of carbons C-4, C-3, and C-5, respectively. The presence of vicinal hydroxyl groups at C-2 and C-3 in the A ring of compound **1** was supported by the HSQC correlations of the oxymethine proton at δ_{H} 3.01 (1H, d, $J = 9.6$ Hz, H-3) with carbon at δ_{C} 82.8 (C-3), as well as the spin system H₂-1(δ_{H} 3.01)/H-2/H-3 observed in the COSY spectrum. The correlation between the signals at δ_{H} 4.79 (1H, dd, $J = 10.2, 7.5$ Hz, H-7) and δ_{C} 67.9 (C-7) in the HSQC spectrum suggested the presence of a third hydroxyl group at C-7. The correlation of H-5/H₂-6/H-7 in the COSY spectrum established the location of the hydroxyl group at this position. The correlations of the methine proton H-12 (δ_{H} 6.36, d, $J = 1.2$ Hz) with C-9, C-14, and C-15 and H-15 (δ_{H} 2.97, m) with C-12, C-14, C-16, and C-17 in the HMBC spectrum substantiated the attachment of the isopropyl group to *para*-benzoquinone and suggested that the quaternary carbon at δ_{C} 188.0 was linked to C-11.

Based on biosynthetic considerations and chemotaxonomic data, this study provides support for the connection between transfused A/B rings in abietanes of the genus *Medusanthia*, with CH₃-20 β -axial and H-5 α -axial rings [11–13,16–18]. The relative configuration of compound **1** was determined through NOESY correlations and coupling constant analysis (Figure 3). The NOESY correlation with H-2/H₃-19/H₃-20 confirmed the cofacial arrangement of these protons, confirming their β orientation. Furthermore, a coupling constant of 9.6 Hz, consistent with an approximate dihedral angle of 168° between H-2 (ddd, $J = 11.5, 9.6, 4.4$ Hz) and H-3 (d, $J = 9.6$ Hz), supported the proposition of a *trans*-diaxial orientation of these protons, indicating an α -axial orientation for H-3. The NOESY correlation of H-5/H-7 confirmed the β orientation of the 7-OH. To corroborate the proposed relative configuration for C-2, C-3, and C-7, ^1H and ^{13}C NMR data for eight isomers (1a–1h) were calculated using the gauge including atomic orbital (GIAO) method at the GIAO-mPW1PW91/6-31+G(d,p) level and then subjected to DP4+ probability analysis. The isomer (2R*,3R*,5R*,7S*,10S*)-1h exhibited a DP4+ probability of 100% (Figure S150). The absolute configuration was determined by comparing the experimental and calculated ECD data and was assigned as 2R,3R,5R,7S,10S (Figure 4). Thus, compound **1** was identified as a new abietane named medusanthol A.

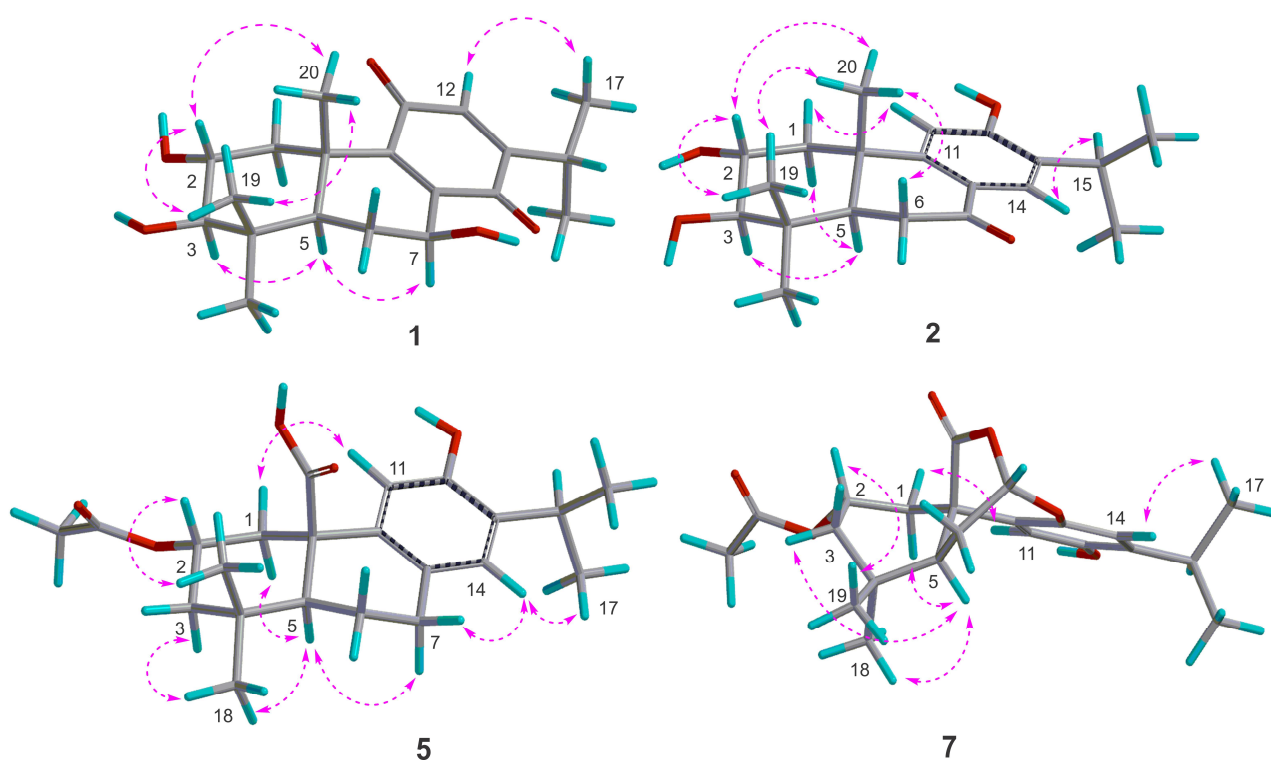


Figure 3. Key ^1H - ^1H NOESY (—) of compounds **1**, **2**, **5**, and **7**.

Compound **2** was obtained as a white amorphous powder and exhibited a molecular formula of $\text{C}_{20}\text{H}_{28}\text{O}_4$ with seven degrees of hydrogen deficiency, as determined by its HRESIMS peak at m/z 687.3863 [$2\text{M} + \text{Na}$] $^+$ (calcd for $\text{C}_{40}\text{H}_{56}\text{NaO}_8$, 687.3867, $\Delta = 0.6$ ppm). The IR spectrum showed bands attributed to hydroxyl groups (3448 cm^{-1}), conjugated keto carbonyl groups (1658 cm^{-1}), and aromatic rings (1595 and 1460 cm^{-1}). The ^{13}C NMR spectrum exhibited 20 carbon signals (Table 1), including resonances assigned to one conjugated keto carbonyl carbon (δ_{C} 200.6), six aromatic carbons (two sp^2 methine carbons at δ_{C} 110.6 and 127.3), two sp^3 methine carbons (δ_{C} 50.3 and 27.9), and five methyl groups, as shown in Table 1. In the ^1H NMR spectrum, a septet at δ_{H} 3.22 (1H, $J = 6.8$ Hz, H-15) and two doublet methyl groups at δ_{H} 1.19 (3H, d, $J = 6.8$ Hz, H-16) and 1.21 (3H, d, $J = 6.8$ Hz, H-17) suggested the presence of an isopropyl group characteristic of the diterpene abietane. Furthermore, the singlets at δ_{H} 6.76 (1H, H-11) and 7.80 (1H, H-14) were assigned to the *para*-aromatic hydrogens of the tetrasubstituted C ring (Table 2).

Analysis of the NMR data of compound **2** indicated a close resemblance to **6**, identified as 2α -hydroxysugiol, a recognized aromatic abietane [19]. The only distinction between the two compounds was the replacement of a methylene carbon signal at δ_{C} 50.4 in C-3 with an oxymethine carbon at δ_{C} 83.5, suggesting the presence of an additional hydroxyl group at this position in compound **2**. In the HMBC spectrum, the correlation between δ_{H} 1.06 and 0.98 (6H, s, H₃-18/H₃-19) and C-3 (δ_{C} 83.5) confirmed the presence of the proposed connectivity (Figure 2). Similar to medusanthol A (**1**), compound **2** also contained vicinal hydroxyl groups attached to C-2 (δ_{C} 69.4) and C-3 (δ_{C} 83.5). Additionally, the correlation between the signal at δ_{H} 7.80 (1H, s, H-14) and the carbon at δ_{C} 200.6 in the HMBC spectrum confirmed the insertion of the carbonyl group at C-7. The NOESY correlations were consistent with the same relative configuration as medusanthol A (**1**). The NOESY correlations of H-2/H₃-19/H₃-20 and H-3/H-5, as well as the coupling constant $^3J_{\text{H-2}/\text{H-3}} = 9.2$ Hz, suggested that H-2/H₃-19/H₃-20 were β -oriented, while H-3/H-5 adopted the α orientation (Figure 3). NMR shift calculations and DP4+ probability analysis supported the relative configuration assigned, with 100% probability ascribed to the $2\text{R}^*,3\text{R}^*,5\text{R}^*,10\text{S}^*-2\text{b}$ isomer (Figure S153). The absolute configuration was determined by comparing the experimental and calcu-

lated ECD data, and the products were assigned as 2*R*,3*R*,5*R*,10*S* (Figure 4). Accordingly, compound **2** was designated medusanthol B.

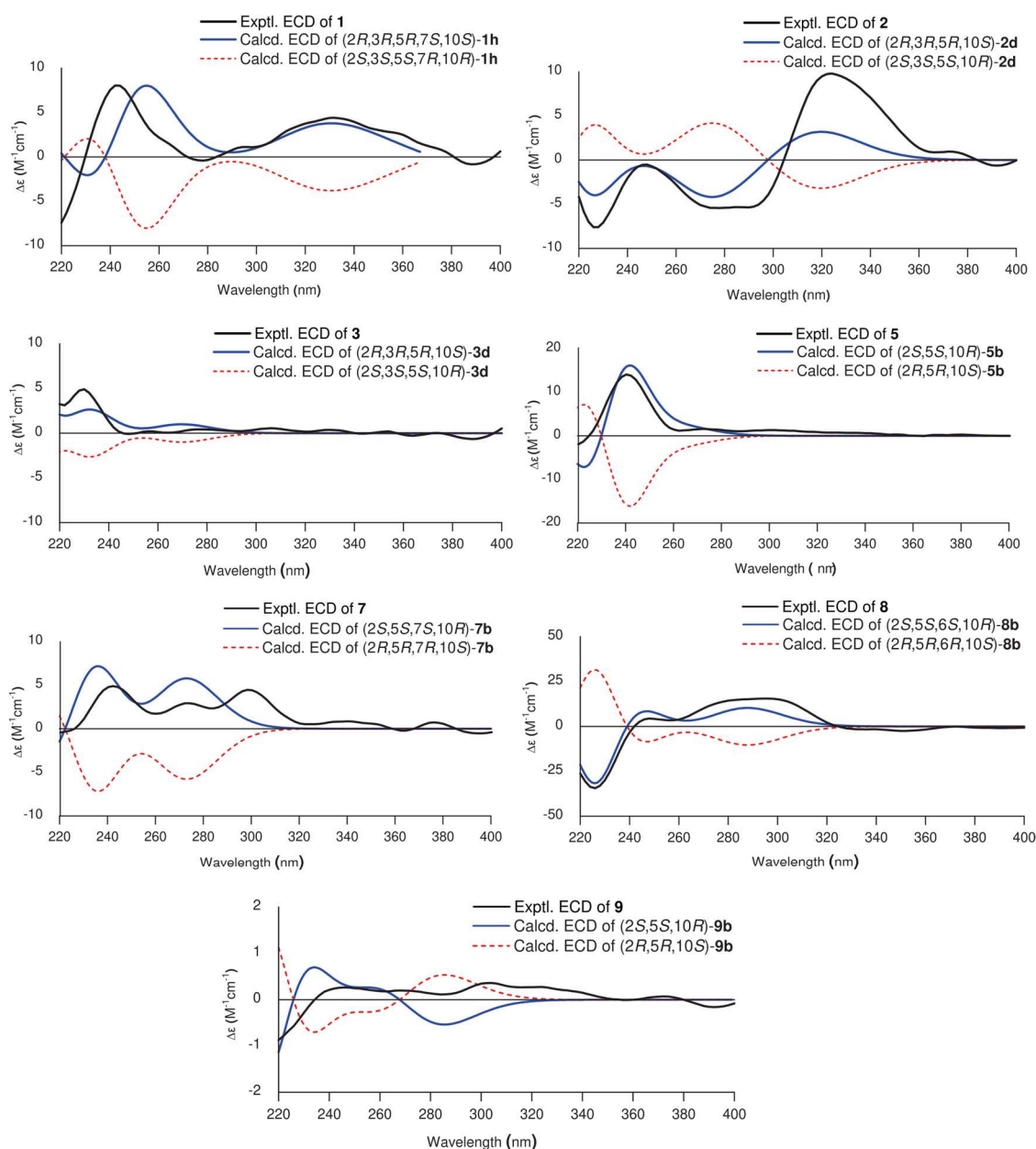


Figure 4. Comparison of experimental and calculated ECD curves of compounds **1–3**, **5**, and **7–9**.

Compound **3**, a needle crystal, was shown to have a molecular formula of $C_{20}H_{30}O_2$ according to its HRESIMS peak at m/z 659.4276 ($[2M + Na]^+$, calcd for $C_{40}H_{60}NaO_6$, 659.4282, $\Delta = 0.9$ ppm), indicating six degrees of hydrogen deficiency. In the IR spectrum, characteristic absorption bands were observed for a hydroxyl group (3361 cm^{-1}) and an aromatic ring (1618 and 1425 cm^{-1}). The 1D and 2D NMR data revealed that compound **3** is also an aromatic abietane, displaying significant structural similarity to medusanthol B (**2**), except for the substitution of the carbonyl group at δ_C 200.6 for the methylene carbon at δ_C 31.1 in C-7 (Table 1). In the 1H NMR spectrum, the shielding of the aromatic proton H-14 (δ_H 6.75, 1H, s) compared to that of medusanthol B (**2**) (Table 2), along with the cross-peak of H-14 with C-7 (δ_C 31.1) in the HMBC spectrum, supported the absence of a carbonyl group at C-7 (Figure 2).

Further comprehensive analysis of the NMR data revealed that compound **3** shares an identical planar structure with 2,3-dihydroxyferruginol, which was isolated from the leaves of *Podocarpus nagi* [20]. The only distinction between these compounds is observed in the configuration at the C-2 center, suggesting a potential stereoisomer. In the NOESY spectrum, correlations between H-2 and H₃-19/H₃-20, along with those between H-3 and H-5/H₃-18, allowed the determination of the α orientation of the 2-OH in compound **3**, which contrasts with the β orientation reported for this group in 2,3-dihydroxyferruginol. Furthermore, the 9.6 Hz coupling constant between H-2 and H-3 in compound **3** is distinct from the 2.9 Hz observed for these protons in 2,3-dihydroxyferruginol, further substantiating the aforementioned proposition. NMR calculations and DP4+ analyses supported the relative configuration of **3** as 2R*,3R*,5R*,10S*-3b with a probability of 100% (Figure S156). Ultimately, the absolute configuration was determined to be 2R,3R,5R,10S by comparing the experimental and calculated ECD data (Figure 4), suggesting that **3** is an epimer of 2,3-dihydroxyferruginol. Biogenetically, the configuration of **3** is proposed to be the same as that of **1** and **2**. Therefore, compound **3** was identified as a new abietane named medusanthol C.

Compound **5**, a white amorphous powder, exhibited a molecular formula of C₂₂H₃₀NaO₅ (m/z 397.1974 [M + Na]⁺, calcd for C₂₂H₃₀NaO₅, 397.1985, Δ = 2.8 ppm), suggesting the presence of an aromatic abietane with eight degrees of hydrogen deficiency. The infrared spectrum displayed characteristic absorptions at 3431 cm⁻¹ (hydroxyl), 1735 and 1269 cm⁻¹ (ester), 1710 cm⁻¹ (carboxylic acid), and 1658, 1510, and 1421 cm⁻¹ (aromatic ring). The ¹³C NMR data of the compound indicated a significant resemblance to medusanthol C (**3**) (Table 1). However, the presence of a single oxygenation on ring A for compound **5** was suggested by the replacement of the oxymethine carbon at δ_C 84.3 (C-3) in medusanthol C with a methylene carbon at δ_C 47.7. Furthermore, the 1D NMR spectrum revealed the deshielding of the oxymethine proton H-2 (δ_H 5.42, 1H, tt, J = 11.7, 4.5 Hz), as well as the presence of characteristic signals for an acetoxy group at δ_H 2.02 (3H, s), δ_C 21.4, and δ_C 172.6 (Tables 1 and 2). This finding was consistent with the presence of a 2-OCOCH₃ group in **5**, similar to miltiorin A, which is isolated from the roots of *Salvia miltiorrhiza* [21]. In the HMBC spectrum, the correlation between the signals at δ_H 1.02 and 0.93 (6H, s, H₃-18/H₃-19) and the signal at δ_C 47.7 assigned to C-3 confirmed the absence of a hydroxyl group at this position (Figure 2). According to the ¹³C NMR spectrum, compound **5** also differed from compound **3** in that it displayed signals for only four methyl groups, indicating the absence of a signal corresponding to CH₃-20, as observed for compound **3** (δ_C 26.3). Therefore, the presence of a signal at δ_C 179.0 was attributed to C-20, indicating oxidation to a carboxylic acid at this position. The HMBC correlations of H-1 (δ_H 3.09, 1H, ddd, J = 12.1, 4.5, 2.8 Hz) with C-2 (δ_C 70.8) and C-20 (δ_C 179.0) confirmed the localization of the acetoxy and carboxylic acid functionalities, respectively (Figure 2).

The relative configuration of **5** was proposed by the NOESY correlations. The NOESY cross peaks of H-2/H₃-19, H-1(δ_H 3.09)/H₃-19, H-1(δ_H 3.09)/H-11 and H-5/H₃-18 indicated that H-2 and CH₃-19 were β -oriented, whereas CH₃-18 and H-5 were α -oriented (Figure 3). NMR calculations and DP4+ analysis confirmed that the relative stereochemistry of the C-2 center was 2S*, with a probability of 100% (Figure S162). The absolute configuration of compound **5** was determined by ECD analysis. The experimental ECD spectrum matched well with the calculated curve (Figure 4), defined as (2S,5S,10R). Thus, **5** was designated medusanthol D.

Compound **7** was obtained as a white amorphous powder with a molecular formula of C₂₂H₂₈O₆, as determined by its HRESIMS peak at m/z 799.3652 [2M + Na]⁺ (calculated for C₄₄H₅₆NaO₁₂, 799.3664, Δ = 1.5 ppm), implying nine degrees of hydrogen deficiency. The IR spectrum displayed characteristic bands for hydroxyl (3446 cm⁻¹) and lactone (1741 cm⁻¹) groups. The 1D and 2D NMR data of **7** showed similarities to those of medusanthol D (**5**), with an acetoxy group at C-2, a tetra-substituted aromatic ring, and four methyl groups in its structure, as shown in Table 1. However, differences between the two compounds were also detected. The ¹H NMR and HSQC spectra of compound **7** revealed an extra

oxymethine signal at δ_{H} 5.94 (1H, d, $J = 6.5$ Hz) and correlations for only three methylene hydrogen groups. Similarly, the HMBC correlation of the signal at δ_{H} 1.85 (1H, t, $J = 11.7$ Hz, H-1) with the carbon at δ_{C} 170.9 suggested oxidation at the C-20 position, consistent with a lactone carbonyl [22] (Figure 2). In particular, the data of **7** notably differed from those of **5** due to the presence of a carbon at δ_{C} 95.4 and the deshielding of C-8 ($\Delta\delta_{\text{C}} + 17.1$ ppm) (Table 1).

Moreover, the correlation between δ_{H} 5.94 and δ_{C} 95.4 in the HSQC spectrum, along with the spin system H-5/H₂-6/H-7 as determined by the COSY spectrum, provided substantial evidence for the presence of an acetal group at C-7. The aforementioned data, along with the HMBC correlations of the acetalic hydrogen H-7 (δ_{H} 5.94, d, $J = 6.5$ Hz) and resonances at δ_{C} 50.6 (C-5), δ_{C} 145.8 (C-8), and δ_{C} 170.9 (C-20), established the C-20-O-C-7 and C-7-O-C-8 connections, confirming a δ -lactone ring between C-20 and C-7 and an acetal functional group at C-7 with ring closure via C-8 (Figure 2).

The relative stereochemistry of compound **7** was deduced from NOESY correlations, similar to those observed for medusanthol E (**5**). The cross-peaks between H-2/H₃-19 and H-5/H₃-18 in the NOESY spectrum suggested that H-2 and H₃-19 adopted a β orientation, while CH₃-18 and H-5 assumed an α orientation (Figure 3). To further determine the relative configuration of compound **7**, the NMR data of two candidates (**7a** and **7b**) were calculated. DP4+ analyses indicated that (2S*,5S*,7S*,10R*)-**7b** was highly likely at 99.81% (Figure S168). Furthermore, the absolute configuration of **7** was determined to be 2S,5S,7S,10R through comparison of the experimental and calculated ECD spectra (Figure 4). Ultimately, **7** was denominated medusanthol E.

Compound **8** was isolated as a white amorphous powder with the molecular formula C₂₂H₂₆O₆, as deduced from its HRESIMS signal at m/z 409.1612 [M + Na]⁺ (calcd for C₂₂H₂₆NaO₆, 409.1622, $\Delta = 2.3$ ppm), corresponding to ten degrees of hydrogen deficiency. In the IR spectrum, characteristic absorption bands for hydroxyl (3446 cm⁻¹), lactonic (1786 cm⁻¹), ester (1720 cm⁻¹), and conjugated ketone (1695 cm⁻¹) groups were observed. The ¹³C NMR spectrum of **8** showed signals between δ_{C} 189.1 and 111.0, similar to those observed for compound **2**, which were attributed to the aromatic carbons of the C ring and the carbonyl of the ketone at C-7 (Table 1). On the other hand, compound **8** also exhibited structural similarities to compound **7**, as evidenced by the signals detected at δ_{C} 176.0 and δ_{C} 66.4, suggesting the presence of a lactone group at C-20 and an acetoxy group at C-2, respectively. In addition, the signals at δ_{C} 22.3, 22.4, 22.7, and 31.4, corresponding to the four methyl groups, also align with those found in compound **7**. However, the absence of signals at δ_{C} 95.4 and 145.8 and the presence of a signal at δ_{C} 81.4 in the ¹³C NMR spectrum of **8** suggested the formation of a lactonic ring via C-20 and C-6, supporting the keto carbonyl at C-7 (δ_{C} 189.1). The shielding of the oxymethylene hydrogen signal from δ_{H} 5.94 (1H, d, $J = 6.5$ Hz, H-7) in **7** to δ_{H} 4.77 (1H, s, H-6) in conjunction with the signal at δ_{C} 81.4 (C-6) in the HSQC spectrum was consistent with the proposed lactonization of **8**. The HMBC correlations of H-6 (δ_{H} 4.77) with signals at δ_{C} 34.0 (C-4), δ_{C} 49.2 (C-10), δ_{C} 121.8 (C-8), and δ_{C} 176.0 (C-20) confirmed that the bridge between C-20 and C-6 formed a γ -lactone ring (Figure 2).

The relative stereochemistry of C-6 was determined by analyzing the dihedral angle between singlets H-5 (δ_{H} 2.41, 1H) and H-6 (δ_{H} 4.77, 1H). These protons displayed an approximately 90° dihedral angle, indicating a pseudoequatorial arrangement for H-6, while H-5 exhibited an α -axial disposition. However, the relative configuration of the C-2 chiral center could not be conclusively determined by NOESY. In this way, the quantum GIAO method was utilized to calculate the ¹³C and ¹H NMR chemical shifts of two potential isomers, (2R*,5S*,6S*,10R*)-**8a** and (2S*,5S*,6S*,10R*)-**8b**. Subsequently, comparison of these computed values with experimental data through DP4+ probability analysis indicated that the most likely relative configuration was (2S*,5S*,6S*,10R*)-**8b**, with a 76.92% probability (Figure S171). To determine the absolute configuration, the calculated and experimental ECD data were compared (Figure 4). The calculated ECD spectrum of **8b** aligned closely

with the experimental curve for **8**, suggesting the absolute configuration of 2*S*,5*S*,6*S*,10*R*. Ultimately, its structure was denoted as medusanthol F.

Compound **9** was obtained as a yellow amorphous powder, with an HRESIMS peak at m/z 799.3637 $[2M + Na]^+$ (calcd for $C_{44}H_{56}NaO_{12}$, 799.3664, $\Delta = 3.4$ ppm), indicating a molecular formula of $C_{22}H_{28}O_6$ and suggesting nine degrees of hydrogen deficiency. The infrared spectrum exhibited absorption bands for hydroxyl (3427 cm^{-1}), lactonic (1791 cm^{-1}), and aldehydic (1724 cm^{-1}) groups. ^{13}C NMR analysis of compound **9** indicated similar chemical shifts in the A ring to those of compounds **5–8**. However, differences in the chemical shifts of the B and C rings were observed compared to those of compounds **1–8** identified in this study (Table 1). According to the ^{13}C NMR and DEPT spectra of compound **9**, six aromatic carbons were identified, including two oxygenated carbons at δ_{C} 150.2 and 146.6, two methine carbons at δ_{C} 110.8 and 108.6, and two nonhydrogenated carbons at δ_{C} 137.1 and 128. Furthermore, the resonance observed at δ_{C} 177.9 in the ^{13}C NMR spectrum was assigned to C-20, indicating the presence of a lactone carbonyl in **9**. In the HMBC spectrum, the correlation of the signal at δ_{H} 3.16 (1H, sept., $J = 6.9$ Hz, H-15) with the signals at δ_{C} 108.6 and 150.2 confirmed the chemical shifts of C-12 and C-14, respectively (Figure 2). Consequently, the HSQC correlation between the proton at δ_{H} 6.57 (1H, s) and the carbon at δ_{C} 110.2, as well as the signal at δ_{H} 6.86 (1H, s) with the carbon at δ_{C} 108.6, confirmed the chemical shifts of the two hydrogenated aromatic carbons at C-8 and C-12, respectively. According to the information provided, it is suggested that the lactone ring in compound **9** formed via the C ring. HMBC correlations from H-8 (δ_{H} 6.57, 1H, s) to C-14 (δ_{C} 150.2), C-11 (δ_{C} 146.6), C-13 (δ_{C} 137.1), C-9 (δ_{C} 128.3), and C-10 (δ_{C} 53.1) confirmed that C-9, C-10, C-11, and C-20, along with an oxygen atom, formed a γ -lactone ring (Figure 2).

In addition, the presence of a signal at δ_{H} 9.19 (1H, t, $J = 1.5$ Hz) in the ^1H NMR spectrum, along with the correlation of this proton with the carbon at δ_{C} 199.5 in the HSQC spectrum, suggested the presence of an aldehydic group in **9**. The correlation of the aldehydic proton (δ_{H} 9.19, 1H, t, $J = 1.5$ Hz) and H-5 (δ_{H} 2.34, 1H, dd, $J = 6.1, 4.6$ Hz) with the C-6 carbon (δ_{C} 41.8) in the HMBC spectrum (Figure 2), along with the COSY spin system H-5/H-6/H-7, determined the position of the aldehyde group at C-7. The conjunction of these correlations established that **9** is a 7-8-*seco*-abietane.

For the same reason as mentioned for compound **8**, the relative configuration of C-2 in **9** was proposed using quantum GIAO NMR chemical shift calculations and DP4+ analysis. The ^{13}C and ^1H NMR data of two possible isomers, (2*R**,5*S**,10*R**)-9a and (2*S**,5*S**,10*R**)-9b, were calculated. The DP4+ probability assessment indicated that the (2*S**,5*S**,10*R**)-9b isomer was highly probable, at 100% (Figure S174). To determine the absolute configuration of **9**, the experimental and calculated ECD results were compared, and **9** was identified as 2*S*,5*S*,10*R* (Figure 4). Ultimately, compound **9** was named medusanthol F.

Furthermore, the structures of the identified known diterpenoids, salviol (**4**) [23] and 2 α -hydroxysugiol (**6**) [19], were confirmed by comparing their spectroscopic data with reported values in the literature. Here, we present the 1D NMR, HRESIMS, ECD, and IR data, along with ^{13}C and ^1H NMR calculations and DP4+ probability analysis for compounds **4** and **6** (see Supplementary Materials).

2.2. Biological Activity

Anti-Neuroinflammatory Activity

Neuroinflammation is characterized by the prolonged activation of glial cells and the influx of immune cells into the nervous system and plays a significant role in the progression of neurodegenerative disorders such as Alzheimer's disease, Parkinson's disease, amyotrophic lateral sclerosis, and traumatic brain injury [24]. Research has shown that abietanes in the Lamiaceae family have the potential to reduce neuroinflammation and act as antioxidants [25,26].

The noncytotoxic concentrations of compounds **1–7** in BV2 cells were determined using the MTT assay. Our results showed that at 50 μM , most compounds reduced cell

viability by more than 20%. On the other hand, at 12.5 and 25 μM , cell viability greater than 80% was observed for all the compounds (Table 3). Therefore, 12.5 μM was considered a safe concentration for assessing the anti-neuroinflammatory effects of compounds 1–7.

Table 3. Cell viability (%) of BV2 cells treated with compounds 1–7.

Compound	Cell Viability (%)		
	12.5 μM	25 μM	50 μM
1	87.95 \pm 2.57	85.09 \pm 1.54	76.28 \pm 2.16
2	81.93 \pm 0.65	85.84 \pm 0.85	74.95 \pm 3.11
3	87.39 \pm 2.35	82.19 \pm 0.96	76.37 \pm 3.14
4	92.29 \pm 0.60	85.41 \pm 0.82	73.61 \pm 2.73
5	86.18 \pm 4.53	86.80 \pm 2.52	82.90 \pm 3.63
6	85.71 \pm 1.11	81.71 \pm 1.37	66.81 \pm 3.61
7	82.74 \pm 0.62	84.91 \pm 1.40	81.83 \pm 1.24

Results are expressed as the mean \pm SEM ($n = 5$) of two independent experiments.

The anti-neuroinflammatory effects of compounds 1–7 were initially evaluated by determining the levels of nitrite, a stable metabolite of NO. As shown in Figure 5, the LPS/IFN- γ -induced inflammatory response was greater in the control group than in the basal group (unstimulated). At 12.5 μM , compounds 1–4 and 7 significantly reduced nitrite levels compared to those in the control group. No significant effect was recorded for compounds 5 and 6. As expected, the positive control quercetin (20 μM) also significantly reduced nitrite levels in stimulated BV2 cells. Nitric oxide plays a crucial role in inflammation, including its involvement in neurodegenerative diseases [27]. Thus, our results suggest that compounds 1, 2, 3, 4, and 7 exert anti-neuroinflammatory effects.

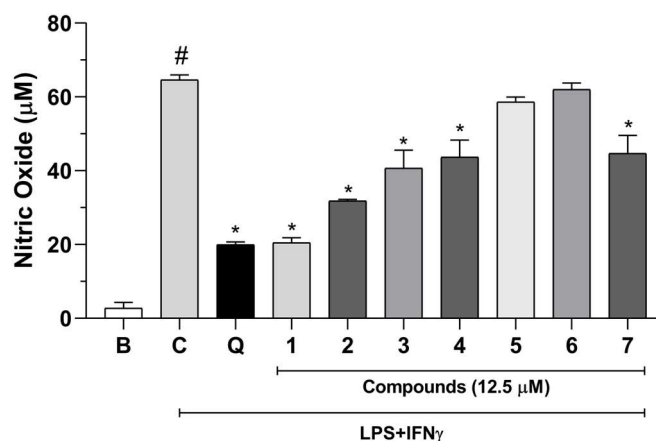


Figure 5. Effects of compounds 1–7 (12.5 μM) on the nitric oxide measurement in LPS and IFN- γ -stimulated BV2 cells. Results are expressed as the mean \pm SEM ($n = 5$) of two independent experiments. B: basal. C: control. Q: quercetin (positive control, 20 μM). # $p < 0.05$ versus basal group; * $p < 0.05$ versus control group.

Considering the promising results for compounds 1 and 2, a new set of experiments was performed to calculate the IC_{50} values at concentrations of 3.125, 6.250, 12.5, and 25 μM . Compounds 1 and 2 exhibited IC_{50} values of 3.12 and 15.53 μM , respectively (Table 4). The IC_{50} value for the positive control quercetin was 11.8 μM . These results support the potent anti-neuroinflammatory effect, especially for compound 1. Moreover, considering that TNF- α acts as an important inflammatory mediator [28], the inhibitory effects of compounds 1 and 2 on LPS- and IFN- γ -induced TNF- α release from BV2 cells were assessed.

Table 4. The IC₅₀ values of compounds 1 and 2 on nitric oxide production inhibition in LPS and IFN- γ -stimulated BV2 cells.

Compound	IC ₅₀ (μ M) ²
1	3.12 \pm 0.75
2	15.53 \pm 7.56
Quercetin ¹	11.8 \pm 1.5

¹ IC₅₀ means half maximal (50%) inhibitory concentration. Results are presented as the mean \pm SEM (95% confidence interval). ² Quercetin was used as positive control.

Compounds 1 and 2 significantly reduced TNF- α levels in stimulated BV2 cells compared to those in the control group (Figure 6). Data from the literature have shown that inflammation induced in BV2 cells increases the activation of signaling pathways such as the NF- κ B and MAPK pathways, leading to the production of cytokines, including TNF- α [29]. TNF- α is a proinflammatory cytokine that modulates the immune system and plays a role in all types of inflammatory disorders, such as central nervous system disorders [30]. Therefore, the anti-neuroinflammatory effects of compounds 1 and 2 are linked to the inhibition of NO and TNF- α release from BV2 cells.

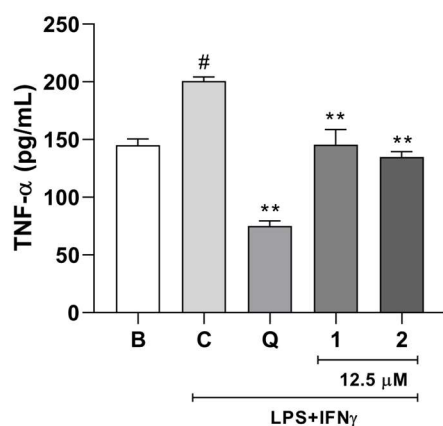


Figure 6. Effects of compounds 1 and 2 (12.5 μ M) on TNF- α measurement in LPS and IFN- γ -stimulated BV2 cells. Results are expressed as the mean \pm SEM ($n = 5$). B: basal. C: control. Q: quercetin (positive control, 20 μ M). # $p < 0.01$ versus basal group; ** $p < 0.01$ versus control group.

3. Experimental Section

3.1. General Experimental Procedures

Optical rotations were measured on a JASCO P-2000 polarimeter (JASCO, Tokyo Japan). Infrared (IR) spectra were recorded on a Shimadzu IRPrestige-21 spectrometer (Shimadzu, Kyoto, Japan) using the KBr disk method. NMR data were acquired on Bruker Ascend 400 MHz and Bruker AvanceNeo 500 MHz spectrometers (Bruker, Billerica, MA, USA) using the residual nondeuterated solvent peaks as an internal standard. The experimental ECD spectra were obtained on a JASCO J-1100 CD Spectrometer (JASCO, Tokyo Japan). The vacuum-liquid chromatography (VLC) system was constructed in a Büchner funnel, and an Erlenmeyer flask was connected to a vacuum system using silica gel (60–200 μ m, 70–230 mesh, SiliaCycle, Quebec, QC, Canada) as the packing material. High-resolution electrospray ionization mass spectrometry (HRESIMS) analyses were carried out using a Bruker micrOTOF II spectrometer (Bruker, Billerica, MA, USA) operating in positive mode. Analytical high-performance liquid chromatography (HPLC) was performed on a Prominence Shimadzu instrument (Shimadzu, Kyoto, Japan) equipped with an SPD-M20A diode array detector and a YMC C-18 (250 mm \times 4.6 mm \times 5 μ m) column. Semipreparative HPLC separations were conducted on a Shimadzu 10AVP instrument (Shimadzu, Kyoto, Japan) with an SPD-M10AVP detector on a Venusil XBP C-18 (259 mm \times 10 mm \times 10 μ m)

column. For preparative HPLC isolations, a Shimadzu apparatus with an SPD-M10A diode array detector and a YMC-Triart® C-18 (250 mm × 20 mm × 5 μm) column was used.

3.2. Plant Material

The aerial parts of *Medusantha martiusii* (Benth.) Harley and J. F. B. Pastore were collected in July 2019 at Maturéia, a Caatinga region of Paraíba, Brazil (07°16'01" S, 37°21'05" W). The sample was authenticated by Maria de Fátima Agra. A specimen is housed under the code JPB 37884 at the Herbarium Prof. Lauro Pires Xavier (JPB) at the Federal University of Paraíba (UFPB), Brazil. This species was registered under the code AB7F3C9 in the National System for the Management of Genetic Heritage and Associated Traditional Knowledge (SisGen-Brasil).

3.3. Extraction, Isolation, and Purification Process

The dried and pulverized aerial parts of *M. martiusii* (1.2 kg) were macerated in hexane four times (4 L) and then in 96% ethanol (4 L) five times, with each cycle lasting 72 h. The filtrates were concentrated under reduced pressure, producing 17.5 g and 43.3 g of hexanic and ethanolic extract, respectively. The hexanic extract (10.0 g) was fractionated by vacuum liquid chromatography using a solvent gradient of Hex–CHCl₃–EtOAc (20:80:0 → 60:40:0 → 50:50:0 → 40:60:0 → 20:80:0 → 0:0:100, *v/v/v*) to obtain six fractions A–F. Fraction F (400 mg) was subjected to preparative HPLC using the following system: solvent A = Milli-Q water with 0.1% formic acid; solvent B = CH₃CN; elution profile = 0.0–38.0 min (50–62% B); 38.0–60.0 min (62–70% B); YMC-Triart® C-18 column; volume injection 200 μL and flow rate of 8 mL/min to yield compounds **1** (5 mg, *t_R* = 12.2 min), **2** (4 mg, *t_R* = 12.7 min), **6** (2 mg, *t_R* = 21.5 min), **3** (24.1 mg, *t_R* = 29.6 min), **9** (2 mg, *t_R* = 39.3 min), **8** (1.5 mg, *t_R* = 43.3 min), and **7** (1.5 mg, *t_R* = 46.1 min), as well as the F₁ subfraction (62.2 mg, *t_R* = 52.3 min), which contained a mixture of substances. The F₁ fraction was further purified by semipreparative HPLC using the following method: solvent A = Milli-Q water; solvent B = CH₃CN; elution profile = 0.0–80.0 min (50% B); Venusil XBP C-18 column; volume injection 100 μL and flow rate of 3 mL/min to obtain compounds **4** (2.6 mg, *t_R* = 71.5 min) and **5** (10.7 mg, *t_R* = 77.4 min).

3.4. Characterization Data

Medusanthol A (**1**): brown amorphous powder; $[\alpha]_D^{23} - 6.8$ (*c* 0.1, MeOH); IR (KBr) ν_{\max} 3432, 1655, 1640 cm⁻¹; ¹H and ¹³C NMR data, see Tables 1 and 2; HRESIMS *m/z* 331.1896 [M – H₂O + H]⁺ (calcd for C₂₀H₂₇O₄, 331.1904, Δ = 2.2 ppm).

Medusanthol B (**2**): white amorphous powder; $[\alpha]_D^{23} + 6.4$ (*c* 0.1, MeOH); IR (KBr) ν_{\max} 3448, 1658, 1595, 1460 cm⁻¹; ¹H and ¹³C NMR data, see Tables 1 and 2; HRESIMS *m/z* 687.3863 [2M + Na]⁺ (calcd for C₄₀H₅₆NaO₈, 687.3867, Δ = 0.6 ppm).

Medusanthol C (**3**): needle crystal; $[\alpha]_D^{23} + 27.9$ (*c* 0.1, MeOH); IR (KBr) ν_{\max} 3336, 1618, 1425 cm⁻¹; ¹H and ¹³C NMR data, see Tables 1 and 2; HRESIMS *m/z* 659.4276 [2M + Na]⁺ (calcd for C₄₀H₆₀NaO₆, 659.4282, Δ = 0.9 ppm).

Medusanthol D (**5**): white amorphous powder; $[\alpha]_D^{23} + 23.5$ (*c* 0.1, MeOH); IR (KBr) ν_{\max} 3431, 1735, 1269, 1710, 1658, 1510, 1421 cm⁻¹; ¹H and ¹³C NMR data, see Tables 1 and 2; HRESIMS *m/z* 397.1974 [M + Na]⁺ (calcd for C₂₂H₃₀NaO₅, 397.1985, Δ = 2.8 ppm).

Medusanthol E (**7**): white amorphous powder; $[\alpha]_D^{23} - 7.9$ (*c* 0.1, CHCl₃); IR (KBr) ν_{\max} 3446, 1786 cm⁻¹; ¹H and ¹³C NMR data, see Tables 1 and 2; HRESIMS *m/z* 799.3652⁺ (calcd for C₄₄H₅₆NaO₁₂, 799.3664, Δ = 1.5 ppm).

Medusanthol F (**8**): white amorphous powder; $[\alpha]_D^{23} + 5.7$ (*c* 0.1, CHCl₃); IR (KBr) ν_{\max} 3446, 1786, 1720, 1695 cm⁻¹; ¹H and ¹³C NMR data, see Tables 1 and 2; HRESIMS *m/z* 409.1612 [M + Na]⁺ (calcd for C₂₂H₂₆NaO₆, 409.1622, Δ = 2.3 ppm).

Medusanthol G (**9**): yellow amorphous powder; $[\alpha]_D^{23} - 32.8$ (*c* 0.1, CHCl₃); IR (KBr) ν_{\max} 3427, 1791, 1745, 1724 cm⁻¹; ¹H and ¹³C NMR data, see Tables 1 and 2; HRESIMS *m/z* 799.3637 [2M + Na]⁺ (calcd for C₄₄H₅₆NaO₁₂, 799.3664, Δ = 3.4 ppm).

3.5. NMR and ECD Calculations

The three-dimensional molecular structures of the compounds were obtained using ChemSketch software version C25E41 [30]. Stochastic conformational searches were performed for all possible stereoisomers of each compound using the Monte Carlo method and the molecular mechanic force field (MMFF) in SPARTAN'10 software version 1.1.0 [31]. All conformers within a relative free energy window of 10 kcal mol⁻¹ were reoptimized using the B3LYP/6-31G(d) level of theory. The conformations within the energy range of 2.5 kcal mol⁻¹ above the minimum energy conformer, corresponding to more than 90% of the total Boltzmann population, were selected for the GIAO NMR calculations and the simulations of the ECD spectra. To simulate nuclear magnetic shielding, the GIAO-mPW1PW91/6-31+G(d,p) level of theory was used, employing a polarizable continuum model with integral equation formalism (IEF-PCM) to implicitly simulate chloroform as a solvent. The ¹H and ¹³C NMR chemical shifts (δ) were obtained using $\delta_i = \sigma_0 - \sigma_i$ after the calculation of the shielding constant of the tetramethylsilane (σ_0) using the same levels of theory. For the application of the DP4+ method, as recommended by the author, the nuclear magnetic shields for all candidates of each compound were added to the DP4+ Excel spreadsheet [32]. For the ECD simulations, TD-DFT was performed in acetonitrile at the CAM-B3LYP/TZVP level. The IEF-PCM model for acetonitrile was used. The final ECD spectra were obtained based on the weighted average Boltzmann statistics of the selected conformers and plotted using Origin 8 software [33]. All quantum-mechanical calculations were performed using the Gaussian 09 software package [34].

3.6. Anti-Neuroinflammatory Assay

3.6.1. Cell Viability (MTT Assay)

The cytotoxicity of compounds 1–7 was evaluated using the MTT (3-(4,5-dimethylthiazol-2-yl)-2,5-diphenyltetrazolium bromide) assay [35]. The microglial BV2 cell line was obtained from the Rio de Janeiro Cell Bank (BCRJ), Brazil. The cells were cultured in Roswell Park Memorial Institute medium (RPMI; Sigma Aldrich, St. Louis, MO, USA) supplemented with 10% fetal bovine serum (FBS; Gibco, Grand Island, NY, USA) and 1% penicillin-streptomycin (Sigma Aldrich) at 37 °C with 5% CO₂. Cells were seeded into 96-well plates at 1 × 10⁵ cells/mL and incubated overnight. After that, the cells were incubated with compounds 1 to 7 (12.5, 25, or 50 μM) in five replicates for 24 h. Then, 110 μL of the supernatant were removed, and 10 μL of MTT solution (5 mg/mL) (Sigma Aldrich, St. Louis, MO, USA) were added. The plates were further incubated for four hours, followed by the addition of sodium dodecyl sulfate (SDS) (100 μL/well) to dissolve the formazan. Optical densities were measured using a spectrophotometer (BioTek Instruments microplate reader, Sinergy HT, Winooski, VT, USA) at a wavelength of 570 nm.

3.6.2. Nitric Oxide (NO) and TNF- α Measurement

To determine the NO and TNF- α levels, BV2 cells were seeded in 96-well plates (1 × 10⁶ cells/mL) in RPMI medium supplemented with 10% FBS and 1% penicillin-streptomycin in a 5% CO₂ incubator at 37 °C. After four hours, the cells were exposed to LPS (500 ng/mL, Sigma Aldrich) and IFN- γ (5 ng/mL, Thermo Fisher) in the absence or presence of compounds 1 to 7 at a final concentration of 12.5 μM (for NO and TNF- α measurement) or 3.125–25 μM (to calculate the IC₅₀ values on NO production inhibition), in five replicates. Quercetin (20 μM) was used as a positive control. After 24 h, cell-free supernatants were collected for NO quantification using the Griess method [36] or stored at –80 °C for cytokine concentration determination. The TNF- α concentrations in the BV2 cell culture supernatants were assessed via enzyme-linked immunosorbent assay (ELISA) with an Invitrogen kit (Thermo Fisher, Vienna, Austria).

3.6.3. Statistical Analysis

The results are expressed as the mean \pm standard error of the mean (SEM), and group comparisons were conducted using one-way analysis of variance (ANOVA) followed by Tukey's post hoc test ($p < 0.05$).

4. Conclusions

Seven new abietane diterpenoids, comprising medusanthol A–G (1–3, 5, 7–9) and two previously identified analogs (4 and 6), were isolated from the hexane extract of the aerial parts of *Medusantha martiusii*. Compounds 1–4 and 7 exhibited significant anti-neuroinflammatory activity in BV2 microglia. Notably, compound 1 exhibited a potent anti-neuroinflammatory effect with an IC_{50} value of 3.12 μ M, while compound 2 displayed an IC_{50} of 15.53 μ M, effectively decreasing NO levels. Additionally, these compounds also reduced TNF- α levels, suggesting their involvement in pathways that mitigate neuroinflammation. Overall, these results not only emphasize the diversity of diterpenes in Nepetoideae but also establish a foundation for its properties in accordance with its traditional usage, thereby reaffirming the potential of the Caatinga biome in uncovering new bioactive compounds.

Supplementary Materials: The following supporting information can be downloaded at <https://www.mdpi.com/article/10.3390/molecules29122723/s1>: Figures S1–S149: NMR, IR, HRESIMS of compounds 1–9. Tables S1–S12: Comparative analysis of theoretical and experimental 1 H and 13 C NMR data of compounds 1–9. Figures S150–S176: DP4+ data, lowest energy conformer data at the B3LYP/6-31G(d) level, and comparison of experimental and calculated ECD data of compounds 1–9.

Author Contributions: E.B.d.A., M.S.d.S., and J.F.T. conceived and designed the main ideas of this work. J.F.T. and M.S.d.S. led the supervision and administration of the project. M.d.F.A. collected and identified the plant material. J.P.R.e.S. designed the chromatographic separations and isolation. E.B.d.A. carried out the fractionation by vacuum liquid chromatography and the isolation of the compounds by preparative HPLC and wrote the original manuscript. E.B.d.A., M.S.d.S., and J.F.T. carried out structural elucidation using 1D and 2D NMR, IR, and HRESIMS data. M.S.d.S. and J.F.T. contributed to the initial draft and revised the manuscript. R.S.d.A. assisted with the recording of the optical rotation experiment and contributed to conducting the infrared experiment. L.S.A. conducted the HRESIMS experiment and analyzed the results. M.V.S. designed and coordinated the experiments related to the biological studies and analyzed the results concerning anti-neuroinflammatory activity. G.M.W.A. and P.B.A.L. assessed cell viability and conducted the nitric oxide and TNF- α measurement assays. F.M.d.S.J. designed and coordinated the experiments related to the computational studies. L.H.M. performed the theoretical calculations of the 1 H and 13 C NMR chemical shifts, ECD, and DP4+ analyses. M.T.S. analyzed the results related to the computational studies and participated in the manuscript revision. All authors have read and agreed to the published version of the manuscript.

Funding: This study was financed by the Rede Norte-Nordeste de Fitoterápicos (INCT/RENNOFITO/CNPq; Project Number: 46.5536/2014-0).

Institutional Review Board Statement: Not applicable.

Informed Consent Statement: Not applicable.

Data Availability Statement: The authors declare that all relevant data supporting the results of this study are available within the article and its Supplementary Materials.

Acknowledgments: The authors acknowledge Conselho Nacional de Desenvolvimento Científico e Tecnológico (CNPq) and Coordenação de Aperfeiçoamento de Pessoal de Nível Superior-Brasil (CAPES) (Finance Code 001) for support and fellowships. We thank M.F.R., Silva, H.D.S., Souza, and E.F., Silva for collecting the NMR and IR data.

Conflicts of Interest: The authors declare no conflicts of interest.

References

1. Harley, R.M.; Pastore, J.F.B. A Generic Revision and New Combinations in the Hyptidinae (Lamiaceae), Based on Molecular and Morphological Evidence. *Phytotaxa* **2012**, *58*, 1. [[CrossRef](#)]
2. Monteiro, F.K.D.S.; Melo, J.I.M.D. Flora da Paraíba, Brasil: Subfamília Nepetoideae (Lamiaceae). *Rodriguésia* **2020**, *71*, e01762018. [[CrossRef](#)]
3. Bornowski, N.; Hamilton, J.P.; Liao, P.; Wood, J.C.; Dudareva, N.; Buell, C.R. Genome Sequencing of Four Culinary Herbs Reveals Terpene Genes Underlying Chemodiversity in the Nepetoideae. *DNA Res.* **2020**, *27*, dsaa016. [[CrossRef](#)] [[PubMed](#)]
4. Ortiz-Mendoza, N.; Martínez-Gordillo, M.J.; Martínez-Ambriz, E.; Basurto-Peña, F.A.; González-Trujano, M.E.; Aguirre-Hernández, E. Ethnobotanical, Phytochemical, and Pharmacological Properties of the Subfamily Nepetoideae (Lamiaceae) in Inflammatory Diseases. *Plants* **2023**, *12*, 3752. [[CrossRef](#)] [[PubMed](#)]
5. Sun, Y.; Yang, H.-Y.; Huang, P.-Z.; Zhang, L.-J.; Feng, W.-J.; Li, Y.; Gao, K. Abietane Diterpenoids with Anti-Inflammatory Activities from *Callicarpa Bodinieri*. *Phytochemistry* **2023**, *214*, 113825. [[CrossRef](#)] [[PubMed](#)]
6. Kolsi, L.E.; Leal, A.S.; Yli-Kauhaluoma, J.; Liby, K.T.; Moreira, V.M. Dehydroabietic Oximes Halt Pancreatic Cancer Cell Growth in the G1 Phase through Induction of P27 and Downregulation of Cyclin D1. *Sci. Rep.* **2018**, *8*, 15923. [[CrossRef](#)] [[PubMed](#)]
7. Abdissa, N.; Frese, M.; Sewald, N. Antimicrobial Abietane-Type Diterpenoids from *Plectranthus punctatus*. *Molecules* **2017**, *22*, 1919. [[CrossRef](#)] [[PubMed](#)]
8. Tabefam, M.; Farimani, M.M.; Danton, O.; Ramseyer, J.; Kaiser, M.; Ebrahimi, S.N.; Salehi, P.; Batooli, H.; Potterat, O.; Hamburger, M. Antiprotozoal Diterpenes from *Perovskia abrotanoides*. *Planta Med.* **2018**, *84*, 913–919. [[CrossRef](#)] [[PubMed](#)]
9. Agra, M.D.F.; Silva, K.N.; Basílio, I.J.L.D.; Freitas, P.F.D.; Barbosa-Filho, J.M. Survey of Medicinal Plants Used in the Region Northeast of Brazil. *Rev. Bras. Farmacogn.* **2008**, *18*, 472–508. [[CrossRef](#)]
10. Ranzato Filardi, F.L.; Barros, F.D.; Baumgratz, J.F.A.; Bicudo, C.E.M.; Cavalcanti, T.B.; Nadruz Coelho, M.A.; Costa, A.; Costa, D.; Goldenburg, R.; Labiak, P.H.; et al. BFG Brazilian Flora 2020: Innovation and Collaboration to Meet Target 1 of the Global Strategy for Plant Conservation (GSPC). *Rodriguésia* **2018**, *69*, 1513–1527. [[CrossRef](#)]
11. Araújo, E.C.C.; Lima, M.A.S.; Silveira, E.R. Spectral Assignments of New Diterpenes from *Hyptis martiusii* Benth. *Magn. Reson. Chem.* **2004**, *42*, 1049–1052. [[CrossRef](#)]
12. Araújo, E.C.C.; Lima, M.A.S.; Montenegro, R.C.; Nogueira, M.A.S.; Costa-Lotufo, L.V.; Pessoa, C.; Moraes, M.O.; Silveira, E.R. Cytotoxic Abietane Diterpenes from *Hyptis martiusii* Benth. *Z. Für Naturforschung C* **2006**, *61*, 177–183. [[CrossRef](#)]
13. Cavalcanti, B.C.; Moura, D.J.; Rosa, R.M.; Moraes, M.O.; Araújo, E.C.C.; Lima, M.A.S.; Silveira, E.R.; Saffi, J.; Henriques, J.A.P.; Pessoa, C.; et al. Genotoxic Effects of Tanshinones from *Hyptis martiusii* in V79 Cell Line. *Food Chem. Toxicol.* **2008**, *46*, 388–392. [[CrossRef](#)] [[PubMed](#)]
14. Barbosa, A.G.R.; Tintino, C.D.M.O.; Pessoa, R.T.; de Lacerda Neto, L.J.; Martins, A.O.B.P.B.; de Oliveira, M.R.C.; Coutinho, H.D.M.; Cruz-Martins, N.; Quintans, L.J., Jr.; Wilairatana, P.; et al. Anti-Inflammatory and Antinociceptive Effect of *Hyptis martiusii* BENTH Leaves Essential Oil. *Biotechnol. Rep.* **2022**, *35*, e00756. [[CrossRef](#)] [[PubMed](#)]
15. Levy, G.C.; Lichter, R.L.; Nelson, G.L. *Carbon-13 Nuclear Magnetic Resonance Spectroscopy*, 2nd ed.; Wiley & Sons: New York, NY, USA, 1980.
16. Han, D.; Li, W.; Hou, Z.; Lin, C.; Xie, Y.; Zhou, X.; Gao, Y.; Huang, J.; Lai, J.; Wang, L.; et al. The Chromosome-Scale Assembly of the *Salvia rosmarinus* Genome Provides Insight into Carnosic Acid Biosynthesis. *Plant J.* **2023**, *113*, 819–832. [[CrossRef](#)]
17. Lima, K.S.B.D.; Pimenta, A.T.A.; Guedes, M.L.S.; Lima, M.A.S.; Silveira, E.R. Abietane Diterpenes from *Hyptis carvalhoi* Harley. *Biochem. Syst. Ecol.* **2012**, *44*, 240–242. [[CrossRef](#)]
18. Costa-Lotufo, L.V.; Araújo, E.C.C.; Lima, M.A.S.; Moraes, M.E.A.; Pessoa, C.; Silveira, E.R.; Morais, M.O. Antiproliferative Effects of Abietane Diterpenoids Isolated from *Hyptis martiusii* Benth (Labiatae). *Pharmazie* **2004**, *59*, 78–79. [[PubMed](#)]
19. González, A.G.; Herrera, J.R.; Luis, J.G.; Ravelo, A.G.; Ferro, E.A. Terpenes and Flavones of *Salvia cardiophylla*. *Phytochemistry* **1988**, *27*, 1540–1541. [[CrossRef](#)]
20. Zhao, H.; Li, H.; Huang, G.; Chen, Y. A New Abietane Mono-Norditerpenoid from *Podocarpus nagi*. *Nat. Prod. Res.* **2017**, *31*, 844–848. [[CrossRef](#)]
21. Hirata, A.; Kim, S.-Y.; Kobayakawa, N.; Tanaka, N.; Kashiwada, Y. Miltiorins A–D, Diterpenes from Radix *Salviae miltiorrhizae*. *Fitoterapia* **2015**, *102*, 49–55. [[CrossRef](#)]
22. Lin, S.; Zhang, Y.; Liu, M.; Yang, S.; Gan, M.; Zi, J.; Song, W.; Fan, X.; Wang, S.; Liu, Y.; et al. Abietane and C₂₀-Norabietane Diterpenes from the Stem Bark of *Fraxinus sieboldiana* and Their Biological Activities. *J. Nat. Prod.* **2010**, *73*, 1914–1921. [[CrossRef](#)]
23. Zheng, T.-L.; Liu, S.-Z.; Huo, C.-Y.; Li, J.; Wang, B.-W.; Jin, D.-P.; Cheng, F.; Chen, X.-M.; Zhang, X.-M.; Xu, X.-T.; et al. Au-Catalyzed 1,3-Acyloxy Migration/Cyclization Cascade: A Direct Strategy toward the Synthesis of Functionalized Abietane-Type Diterpenes. *CCS Chem.* **2021**, *3*, 2795–2802. [[CrossRef](#)]
24. Zhang, W.; Xiao, D.; Mao, Q.; Xia, H. Role of Neuroinflammation in Neurodegeneration Development. *Signal Transduct. Target. Ther.* **2023**, *8*, 267. [[CrossRef](#)]
25. Oliveira, M.R. The Dietary Components Carnosic Acid and Carnosol as Neuroprotective Agents: A Mechanistic View. *Mol. Neurobiol.* **2016**, *53*, 6155–6168. [[CrossRef](#)] [[PubMed](#)]
26. Oliveira, M.R.; Souza, I.C.C.; Fürstenau, C.R. Carnosic Acid Induces Anti-Inflammatory Effects in Paraquat-Treated SH-SY5Y Cells Through a Mechanism Involving a Crosstalk Between the Nrf2/HO-1 Axis and NF-κB. *Mol. Neurobiol.* **2018**, *55*, 890–897. [[CrossRef](#)] [[PubMed](#)]

27. Justo, A.F.O.; Suemoto, C.K. The Modulation of Neuroinflammation by Inducible Nitric Oxide Synthase. *J. Cell Commun. Signal.* **2022**, *16*, 155–158. [[CrossRef](#)] [[PubMed](#)]
28. Kongsman, J.P. Cytokines in the Brain and Neuroinflammation: We Didn't Starve the Fire! *Pharmaceuticals* **2022**, *15*, 140. [[CrossRef](#)] [[PubMed](#)]
29. Wang, H.; Wang, H.; Wang, J.; Wang, Q.; Ma, Q.; Chen, Y. Protocatechuic Acid Inhibits Inflammatory Responses in LPS-Stimulated BV2 Microglia via NF- κ B and MAPKs Signaling Pathways. *Neurochem. Res.* **2015**, *40*, 1655–1660. [[CrossRef](#)]
30. ChemSketch, Version 2022.1.2; Advanced Chemistry Development, Inc. (ACD/Labs): Toronto, ON, Canada, 2022. Available online: www.acdlabs.com (accessed on 19 October 2023).
31. Spartan' 10, Version 1.1.0; Wavefunction Inc.: Irvine, CA, USA, 2011.
32. Grimblat, N.; Zanardi, M.M.; Sarotti, A.M. Beyond DP4: An Improved Probability for the Stereochemical Assignment of Isomeric Compounds Using Quantum Chemical Calculations of NMR Shifts. *J. Org. Chem.* **2015**, *80*, 12526–12534. [[CrossRef](#)]
33. Origin(Pro), Version 2023; OriginLab Corporation: Northampton, MA, USA, 2023.
34. Frisch, M.J.; Trucks, G.W.; Schlegel, H.B.; Scuseria, G.E.; Robb, M.A.; Cheeseman, J.R.; Scalmani, G.; Barone, V.; Petersson, G.A.; Nakatsuji, H.; et al. *Gaussian 09*; Gaussian, Inc.: Wallingford, CT, USA, 2016.
35. Mosmann, T. Rapid Colorimetric Assay for Cellular Growth and Survival: Application to Proliferation and Cytotoxicity Assays. *J. Immunol. Methods* **1983**, *65*, 55–63. [[CrossRef](#)]
36. Griess, P. Bemerkungen Zu Der Abhandlung Der HH. Weselsky Und Benedikt "Ueber Einige Azoverbindungen". *Berichte Dtsch. Chem. Ges.* **1879**, *12*, 426–428. [[CrossRef](#)]

Disclaimer/Publisher's Note: The statements, opinions and data contained in all publications are solely those of the individual author(s) and contributor(s) and not of MDPI and/or the editor(s). MDPI and/or the editor(s) disclaim responsibility for any injury to people or property resulting from any ideas, methods, instructions or products referred to in the content.